Using Digital Cameras as Quasi-Spectral Radiometers to Study Complex Fenestration Systems

Nicholas Gayeski, MSc, Eleanor Stokes, AB, Marilyne Andersen*, PhD,

Building Technology Program, Department of Architecture, Massachusetts Institute of Technology, Cambridge MA, USA

short title: Using Digital Cameras as Quasi-Spectral Radiometers

* Corresponding author. Address for correspondence: M. Andersen, MIT Building 5-418, 77 Massachusetts Ave, Cambridge MA 02139, USA. Phone: 617-253-7714, Email: mand@mit.edu

Abstract

This work discusses the use of digital cameras used with absorption filters as quasi-spectral radiometers. By filtering incident light into selected wavelength intervals, accurate estimates of radiances can be made for unknown spectra. This approach is being employed as part of a new video-projection goniophotometer to study the properties of angularly and spectrally selective complex fenestration systems (CFS).

Complex fenestration systems are increasingly being used to distribute solar radiation purposefully in buildings. They can be utilized to optimize energy performance and enhance daylighting. Radiance estimates from calibrated digital cameras enable the assessment of quasi-spectral, bi-directional scattering distribution functions (BSDF) of total radiance transmitted or reflected by a fenestration system over desired wavelength intervals. A silicon and an indium gallium arsenide digital camera are used to enable measurements across a 380 to 1700 nm interval.

Nomenclature

a	experimentally determined constant (-.13254)
$a_{\Delta\lambda,filterset}$	fraction of total radiance in a wavelength interval $\Delta\lambda$ assumed for each filter set based on a neutral sample
ASR	Absolute spectral responsivity
b	experimentally determined constant (363.51)
BSDF	Bidirectional Scattering Distribution Function (sr^{-1})
$BSDF_{e,\Delta\lambda}$	Quasi-spectral Bidirectional Scattering Distribution Function (sr^{-1}) over wavelength interval $\Delta\lambda$
$BSDF_{e,380-1700}$	Total BSDF of a sample to a given source across the 380 to 1700 nm interval
c	experimentally determined constant (1.4468e7)
CCD	Charge-coupled device
CFS	Complex fenestration system
d	experimentally determined constant (-.40717)
$DL_{R,G,B}$	digital level in the red, green, or blue channel
$_e$ (subscript)	radiometric units
$E_{e,source}(\lambda)$	spectral exitance of the light source ($\mu W/cm^{2)}$
$E_{,e,\Delta\lambda}(\theta_i)$	directional radiance incident on a sample spanning wavelength interval $\Delta\lambda$

f	f-number of the camera
$H(\lambda)$	spectral exposure of sensor array
$h(\lambda)$	measured spectral exposure given by scene radiance multiplied by integration time ($\mu J/cm^2$-sr)
$h_{R,G,B}^{0.3}(\lambda)$	$h(\lambda)$ resulting in NDL=0.3 for the red, green, or blue channel ($\mu J/cm^2$-sr)
$[1/h_{RGB,filterset}^{0.3}]$	assumed total responsivity of CCD camera for a given filter set based on a neutral sample
HMI	Hydrargyrum medium air iodide
InGaAs	Indium gallium arsenide
k	camera spectral exposure constant
$L_{e,beam,380\text{-}945}$	total radiance in a polychromatic beam for the wavelength interval between 380nm and 945nm ($\mu W/cm^2$-sr)
$L_e(\lambda)$	spectral radiance ($\mu W/cm^2$-sr)
$L_{e,i}(\theta_i,\phi_i,\theta_r,\phi_r)$	bidirectional spectral radiance for filter combination j, ($\mu W/cm^2$-sr)
$L_{,e,\Delta\lambda}(\theta_i,\phi_i,\theta_{t(r)},\phi_{t(r)})$	bi-directional radiance across a wavelength interval $\Delta\lambda$
N	aperture number

$NDL_{R,G,B}$	normalized digital level (digital level divided by 2^8) in the red, green, or blue channel
NIR	Near infrared radiation
$p_{\Delta\lambda}$	fraction of total radiance in a wavelength interval $\Delta\lambda$
$r_{RGB}(\lambda)$	absolute spectral responsivity of CCD camera in the red, green, and blue channel (NDL/(μJ/cm^2-sr))
$r_{RGB,\Delta\lambda}$	discretized absolute spectral responsivity of CCD camera in the red, green, and blue channel (NDL/(μJ/cm^2-sr))
t_{int}	integration time
VC(x,y)	vignetting correction factor as a function of pixel coordinates (x,y)
θ_i	incident altitude angle (radians)
φ_i	incident azimuth angle (radians)
$\theta_{t(r)}$	transmitted or reflected alititude angle (radians)
$\varphi_{t(r)}$	transmitted or reflected azimuth angle (radians)

1. Introduction

In 2004, building energy consumption accounted for 39 percent of total U.S. energy consumption[1]. According to one study, energy use due to fenestration systems through impacts on heating, cooling and lighting demand accounted for about 7 quadrillion BTUS of energy consumption, or about 7 percent of annual U.S. energy consumption[2]. If one existing fenestration technology, low-emissivity glazings, were deployed throughout the residential building market it was estimated that residential heating and cooling energy consumption attributable to windows would drop by about 41 percent[3].

Daylighting systems designed to enhance lighting conditions within spaces have potential impacts on occupant comfort, electrical energy savings and aesthetics. Loftness and Harktopf estimate that 30 to 60 percent of annual lighting energy could be saved through effective daylighting strategies[4]. Daylighting may also improve comfort, human health, productivity, the performance of tasks, and have financial implications, but if implemented poorly may have opposite effects, such as causing glare or overheating[5].

Angularly and spectrally selective fenestrations are one type of complex fenestration system (CFS). These systems can transmit or reflect different parts of the solar spectrum in different directions for different angles of incidence of solar radiation. The potential of this kind of system, for example, is to transmit visible light deeply into spaces throughout the year while reflecting near infrared radiation (NIR) during the summer and transmitting it during the winter. One study showed that angularly selective glazings tuned theoretically for optimal optical properties could reduce annual cooling energy loads by 18 percent and annual electricity use by 15 percent relative to spectrally selective windows, already an improvement over conventional windows[6]. At the same time, they would provide a better daylight distribution.

Accounting for both daylighting and thermal issues in the development of angularly and spectrally selective glazings requires the study of angularly and wavelength dependent optical properties of fenestration systems across the entire spectrum of solar radiation. The ability to study these properties will help in characterizing, modeling and analyzing their performance in the built environment as well as in designing new systems. A new spectral video-goniophotometer is under development at the Massachusetts Institute of Technology (MIT) to meet this need.

The methods developed here for using digital cameras as quasi-spectral radiometers enable video-projection goniophotometers to measure quasi-spectral, bi-direction scattering distribution functions (BSDF). A growing library of BSDFs is useful for daylighting and energy simulations involving complex materials and CFS. The calibrated cameras could also be used separately to conduct thermal and visual assessments of rooms. This is similar to the use of many digital cameras for studying luminance or radiance distributions in rooms[7, 8], except that with the use of filters it could also be used to measure quasi-spectral transmission and reflection properties of surfaces within the room.

2. A Spectral Video-Goniophotometer

Goniophotometers have been widely used to study the optical properties of lamps and luminaires, ground surfaces and ground textures[9] and natural materials such as wood[10]. They are increasingly being used for assessing the bi-directional optical properties of fenestration system materials and components[11]. Only very recently have goniophotometers for fenestration

systems been developed that measure spectral as well as bi-directional dependence[12].

However, existing goniophotometers that provide spectral information utilize detectors to scan the hemisphere of radiation emerging from a sample. The development of quasi-spectral radiance measurement using digital cameras will enable video-projection goniophotometers to measure spectral properties using a video-projection method. This has advantages over scanning goniophotometers because a full hemi-sphere of data can be collected at once, saving time, and spatial averaging prevents missing parts of the distribution due to poor sampling resolution[13,14,15].

The goniophotometer under development at MIT will measure quasi-spectral, BSDF of materials and components used in fenestration systems. The basic components are a 400W Dedolight hydrargyrum medium arc iodide (HMI) source, a rotating sample holder, a projecting device, and a charge coupled device (CCD) and Indium Gallium Arsenide (InGaAs) digital camera[16]. Filters are used to sample the spectrum of the source, isolating wavelength intervals over which radiance estimation can be performed accurately. A schematic of

the device is shown in Figure 1. A more complete description of the video-goniophotometer can be found in other sources[16, 17].

§ Figure 1. MIT Video-Goniophotometer

Filtered radiation impinges on a fenestration sample at the center of the rotating table, coincident with one focal point of the hemi-ellipsoid. After irradiating the sample, radiation is transmitted or reflected into a full hemisphere, reflected off of the hemi-ellipsoid and directed towards its other focal point where it is recorded by a digital camera equipped with a fish eye lens.

The quasi-spectral radiance estimated by the digital camera combined with absorption filters provides the numerator for a quasi-spectral BSDF while the denominator, the irradiance of the sample, is known. An average BSDF across a wavelength interval $\Delta\lambda$ for the radiation source can then be calculated as follows:

$$(1) \qquad BSDF_{e,\Delta\lambda}(\theta_{t(r)}, \varphi_{t(r)}, \theta_i, \varphi_i) = \frac{L_{e,\Delta\lambda}(\theta_{t(r)}, \varphi_{t(r)}, \theta_i, \varphi_i)}{E_{e,\Delta\lambda}(\theta_i)}$$

The full spectral BSDF is entirely independent of the source of radiation, and is a property of the material or system being studied, whereas the quasi-spectral

BSDF defined above depends on the radiation source spectrum, chosen to simulate solar radiation.

3. Camera Calibrations

A critical step in the measurement of quasi-spectral BSDFs is spectroradiometric calibration of the CCD camera and InGaAs NIR digital camera. These calibrations enable the measurement of radiance for unknown spectra reflected or transmitted from spectrally and angularly selective fenestration samples.

The CCD camera is a Kappa DX20 color CCD camera. The InGaAs camera is a Sensors Unlimited SU320 1.7RT camera. A Fujinon FE185C057HA high resolution fisheye lens is used with both cameras. The NIR filter has been removed from the CCD camera to capture wavelengths between 780 and 945 nm. A non-linear gamma of 0.5 was chosen for the CCD camera to enable better differentiation of low luminance features in a single image. Ultimately, the pixels will be averaged over user selected solid units of angle. The integration time, which can range from microseconds to minutes, is varied to capture images of less or more radiance or luminance.

For both cameras a vignetting correction will be applied, in terms of a function VC(x,y) dependent the x,y image coordinates to correct for light drop-off near the end of the image. An angular resolution of 0.0017 steradians for the CCD camera and 0.25 steradians for the InGaAs camera limits the BSDF features distinguishable by each camera. Spatial calibrations for each camera have also been performed relating pixel location to zenithal angle of incidence on the camera. Due to the fish eye lens, the relationship between pixel distance from principal point and zenithal angle is linear and passes through the origin, by definition of principal point[18]. A coefficient of 0.1886 degrees per pixel relates zenith angle to the pixel location relative to the principal point for the CCD camera, whereas the coefficient is 0.7995 degrees per pixel for the NIR camera.

3.1 Spectroradiometric calibration

Spectroradiometric calibration of the digital cameras was performed to relate digital output to the radiance viewed by the camera. The output of a digital camera for a given pixel at a given wavelength is related to the spectral exposure, in units of energy, of the sensor area correlating to that pixel. The spectral exposure is dependent on the number of photons of a given wavelength

impinging on the detector area, which are in turn related to the radiance of the scene viewed by the camera[19]. In its most simple form, the spectral exposure, H(λ) is related to scene spectral radiance by:

$$H(\lambda) = k \frac{L_e(\lambda)}{N^2} t_{int} \quad (2)$$

where *k* is a constant depending on the optical and geometric properties of the imaging system, *N* is the aperture number, t_{int} is the integration time and $L_e(\lambda)$ is spectral radiance[20]. In this application, the f-number of the lens is fixed at f/4, and thus N in equation can be absorbed into the constant k. Furthermore, the digital output for a pixel is physically related to its spectral exposure and can be thought of as a function of the scene radiance, such that:

$$NDL_{R,G,B}(\lambda) = DL_{R,G,B} / 2^8 = f(H(\lambda)) \quad (3)$$

where $NDL_{R,G,B}$ and $DL_{R,G,B}$ are the Normalized Digital Level and Digital Level of the R,G, or B channel.

To study the relationship between spectral exposure and the NDL response of the camera, the camera output was measured against known monochromatic radiances and integration times. The constant of proportionality relating radiance to spectral exposure, k, was not measured. Instead, the relationship between NDL and the product of $L_e(\lambda)$ and t_{int} was measured directly.

A Labsphere KI-120 Illuminator tungsten-halogen lamp, a Spectral Products CM110 monochromator, and a ~99 percent reflective Labsphere Spectralon coated diffusing, reflectance standard were used to create monochromatic radiances for viewing by the camera as shown in Figure 2. Pictures were taken at many integration times, from about one millisecond to many seconds to cover a full range of exposures from below the camera's threshold to above saturation for each wavelength. Spectral radiances of about 0.1 to 1 $\mu W/cm^2$-sr-nm were used for the relative spectral sensitivity calibration.

§ Figure 2. Spectroradiometric experimental schematic

An Ocean Optics USB2000 spectrometer was used to measure the irradiance of the reflectance standard, with known properties used to calculate reflected radiance. These experiments were conducted with monochromatic beams at every 50 nm from 450 nm to 950 nm of about 1 to 50 $\mu W/cm^2$-sr. The shape of these response curves was observed to be the same for each channel and all wavelengths.

The camera response is best approximated by a logistic dose response function, selected from a set of functions that best model the response of digital cameras[20]. This function is the solid line in Figure 3 plotted against all data points.

§ Figure 3. Normalized response for R, G and B channels to many wavelengths fit with a logistic dose response function

The logistic dose response curve for the camera was found to be:

$$NDL_{R,G,B} = a + \frac{b}{1 + \left(\frac{h(\lambda) / h^{0.3}_{R,G,B}(\lambda)}{c} \right)^{d}} \quad (4)$$

with a = -0.13254, b = 363.51, c = 1.4468e7 and d = - 0.40717. Equation (4) can be inverted and solved for the monochromatic radiance viewed by the camera to give the equation:

$$L_e(\lambda) = \frac{h^{0.3}_{R,G,B}(\lambda)}{t_{int}} \times c \left(\frac{b}{(NDL_{R,G,B} - a)} - 1 \right)^{1/d} \quad (5)$$

3.2 Spectral Sensitivity

The spectral sensitivity properties of the camera are contained in the wavelength dependent normalization factor, $h^{0.3}_{R,G,B}(\lambda)$, for each channel. A 5 nm wavelength resolution in the spectral sensitivity is desired to achieve accurate measurements of spectra as explained in (ASTM 2001)[21].

The normalization spectral exposures $h^{0.3}_{R,G,B}(\lambda)$ were determined as follows. Images of monochromatic radiances were taken at the same integration time for each wavelength. The Ocean Optics spectrometer was used to measure the spectral irradiance of the reflectance standard. The monochromatic radiance viewed by the camera was calculated based on the measured irradiance and the reflectance standard's spectral reflection coefficients.

Through the inverted logistic dose response function given by equation (5), the normalized spectral exposures, $h^{0.3}_{R,G,B}(\lambda)$, were calculated from the real digital output of the camera, the normalization digital level, NDL = 0.3, and the measured spectral exposure, or radiance multiplied by integration time. This relation is given by:

$$\frac{h^{0.3}_{R,G,B}(\lambda)}{h_{Measured}(\lambda)} = \frac{c\left(\frac{b}{(0.3-a)}-1\right)^{1/d}}{c\left(\frac{b}{((NDL_{R,G,B,Measured})-a)}-1\right)^{1/d}} \quad (6)$$

where all quantities are known except $h^{0.3}_{R,G,B}(\lambda)$. The inverse of these normalized spectral exposures gives the absolute spectral responsivity (ASR) of each channel[22]. The ASR can be written $r_{R,G,B}(\lambda) = 1/h^{0.3}_{R,G,B}(\lambda)$, where the subscripts denote a different ASR for each channel. It has the units of digital output per unit energy per unit area per solid unit of angle, or NDL/(μJ/cm^2–sr).

An integrating sphere was used to more accurately measure irradiance, as shown in Figure 2, from which radiance was calculated to scale the relative sensitivity of each channel to the correct magnitude. The relative sensitivity of each channel was positioned relative to the integrating sphere measurements such that the sum of the square of the differences between the scaled ASRs and the integrating sphere data points was minimized.

§ Figure 4. Absolute spectral responsivity curves for R, G and B channels scaled to integrating sphere calibration points

The result of this spectral sensitivity calibration is an ASR curve for the R, G and B channels given by $r_{R,G,B}(\lambda) = 1/h^{0.3}_{R,G,B}(\lambda)$ over 5 nm wavelength intervals, rewritten in discrete form as $r_{R,G,B,\Delta\lambda} = 1/h^{0.3}_{R,G,B,\Delta\lambda,}$ spanning 380 to 945 nm as shown in Figure 4. A similar characteristic response and spectral

sensitivity was also measured for the InGaAs camera, as shown in Figure 5, and the same analytical methods apply although they are not discussed in detail here.

§ Figure 5. Absolute spectral responsivity of InGaAs camera

3.3 Response to Polychromatic Radiation

Theoretically, the digital output of the camera stimulated by polychromatic radiation should be related to the total, not spectral, exposure of its sensor array as explained in (Brown et al. 2001) [22]. The total exposure of a pixel is given by the integral of its spectral exposures weighted by that channels ASR, $r_{R,G,B,\Delta\lambda} = 1/h^{0.3}_{R,G,B,\Delta\lambda}$. The digital output of the channel is a function of this total exposure, given by:

$$NDL_{R,G,B} = f\left(\sum_{380-945} r_{R,G,B,\Delta\lambda} L_{e,\Delta\lambda} t_{int}\right) \quad (7)$$

Where the exposure has been written in terms of radiance and integration time and the result is in discrete form. $L_{e,\Delta\lambda}$ is the total radiance over a wavelength interval $\Delta\lambda$ and the sum occurs over all wavelength intervals to which the

camera is sensitive. If the total radiance of the beam across the range to which the camera is sensitive is given by:

$$L_{e,beam,380-945} = \sum_{380-945} p_{\Delta\lambda} L_{e,beam,380-945} \tag{8}$$

where $p_{\Delta\lambda}$ is the fraction of the total radiance from 380 to 945 nm in a wavelength interval $\Delta\lambda$, then equation (8) can be re-written in as:

$$NDL_{R,G,B} = f\left(L_{e,beam,380-945} t_{int} \sum_{380-945} r_{R,G,B,\Delta\lambda} p_{\Delta\lambda} \right) \tag{9}$$

Thus, the absolute responsivity of the camera to a polychromatic beam is simply a weighted sum of the ASRs where the weights are determined by the relative spectra of the beam, given by $p_{\Delta\lambda,}$ across the wavelength interval over which the camera is sensitive. Because the non-linear response of the camera has the same shape for all channels and all wavelengths, the function relating NDL and radiance for a polychromatic beam is the same as that for a monochromatic beam, shown in equation (4). This suggests that the functional form of equation (9) is given by:

$$NDL_{R,G,B} = a + \frac{b}{1 + \left(\frac{(L_{e,beam,380-945} t_{int}) / h_{R,G,B,beam}^{0.3}}{c} \right)^{d}} \tag{10}$$

which has the same form as equation (4) except that the absolute spectral responsivity has been replaced by a polychromatic responsivity given by the weighted sum of absolute spectral responsivities, or:

$$\frac{1}{h^{0.3}_{R,G,B,beam}} = \sum_{380-945} \frac{p_{\Delta\lambda}}{h^{0.3}_{R,G,B,\Delta\lambda}} \tag{11}$$

This can be thought of as the total (not spectral) absolute responsivity of each channel to a polychromatic beam with the relative spectrum given by $p_{\Delta\lambda}$.

The final equation relating the camera's digital output for polychromatic radiation to the total radiance in that beam is given by:

$$L_{e,beam,380-945} = \frac{h^{0.3}_{R,G,B,beam}}{t_{int}} \times c\left(\frac{b}{(NDL_{R,G,B} - a)} - 1\right)^{1/d} \tag{12}$$

where the absolute responsivity of R, G and B to the beam, $1/h^{0.3}_{R,G,B,beam}$, is given by equation (11).

Experiments confirm that this relation holds. The digital response of the camera to polychromatic beams with known radiances was measured using the experimental setup shown in Figure 6.

§ Figure 6. Schematic of the two beam polychromatic response experiment

First, a polychromatic beam made up of two monochromatic beams was imaged. Two monochromatic sources irradiated the Labsphere reflectance standard simultaneously and separately. The spectral irradiance of the standard was measured for each scenario, from which radiance was calculated. The result for the B channel, mixing a 500 and 550 nm beam, is shown in Figure 7.

§ Figure 7. Two beam polychromatic experiment: predicted exposures (Pred) from B channel compared to measured exposures (Meas) for two separate beams (500, 550) and a polychromatic beam (Comb)

The measured points and predicted response curves are shown to match closely, typically better than 5 percent across the range of the camera's response. The polychromatic response function also holds for more typical polychromatic beams, such as a tungsten halogen lamp filtered with a 695 nm longpass filter, as shown in Figure 8.

§ Figure 8. General polychromatic response: camera response to tungsten-halogen lamp with 695 nm long pass filter

3.4 Measuring Radiance of Spectra Altered by Spectrally Selective Fenestrations

In order to use the known polychromatic response of the camera to assess the radiance distribution emerging from spectrally selective fenestration samples it is necessary to filter radiation into sub-intervals over which accuracy can be maintained in radiance estimation. Ignoring speed and operability issues, the simple solution is to filter the spectrum into near monochromatic beams for which the relationship between digital response and radiance is well known. However, this is impractical.

A different method has been developed to accurately measure the net radiometric or photometric transmission or reflection across wavelength intervals of interest, divided into segments of the visible and NIR. This is done by choosing filters which span wavelengths over which the camera's sensitivity is reasonably constant, and alterations in observed spectra result in acceptable radiance estimation errors.

Simulations of the cameras predicted radiance for unknown spectra filtered to span finite wavelength intervals were performed using a wide variety of color

filters. The total radiance across each wavelength interval calculated from the simulated digital output was compared to the true radiance across the interval. Simulations were performed with all possible combinations of Schott short, long and band pass filters listed in the Schott Glass Filter Catalog[23]. Schott Color Glass Filters were chosen because they provided affordable filters with reasonably sharp transitions from absorbing to transmitting over appropriate intervals.

The filter combinations that led to the best predicted radiance and luminance from the camera across each interval for a range of expected fenestration samples was chosen for use with the CCD camera. The optimal filters are shown in Table 1. The filtered spectrum of the HMI lamp used to simulate solar radiation is shown in Figure 9. These filters span larger wavelength intervals where either the R, G, or B channel have gradually changing ASR and span smaller wavelength intervals where the channel ASR have greater slopes. There are also more filters for wavelengths at which the photopic response curve has the greatest slope to achieve greater accuracy in luminance measurements.

§ Figure 9. Unfiltered HMI lamp spectrum and the filtered HMI lamp spectra for each of the eight filter combinations listed in Table 1

§ Table 1. Filter Specifications

To quantify the accuracy of radiance measurement, the spectrum viewed by the camera for each filter set was altered systematically by assuming a fenestration sample with linearly increasing or decreasing spectral transmission or reflection coefficients. These variations changed by defined amount over a defined wavelength interval, as shown in figure 9 for filter set 3.

§ Figure 10. The effect of linearly varying hypothetical transmission coefficients, shifted across the filtered spectra, were studied to calculate the theoretical accuracy of using each filter set to estimate radiance and luminance across a given band.

The errors introduced by using the camera to estimate the radiance of unknown spectra for each filter set were calculated. Note that *some* knowledge of the spectrum is assumed, that is, the spectrum viewed by the camera is assumed to be altered from an expected spectrum (the filtered HMI spectrum). Each channel's responsivity to the expected spectrum, given by equations (11) and (12), is used to calculate radiance. The error between the radiance calculated

using this responsivity was compared to the true radiance of the altered spectrum.

The error analysis provides limits on how much a spectrum can be altered from the expected spectrum within each wavelength interval such that the camera can still measure radiance or luminance accurately. As shown in Table 2, alterations to the spectrum were defined that introduce errors in radiance estimation by no more than about 13 percent. Errors in luminance estimation were introduced to maintain accuracy of 10 percent in the dominant regions of the photopic curve, and no more than 25 percent for less sensitive regions, such as the deep blue and red.

Table 2 shows the maximum allowable HMI spectrum alterations, and thus constraints on fenestration sample spectral transmission or reflection properties, by the magnitude of the change in spectral properties (Percent Change in R or T) over a wavelength interval (Variation Interval).

§ Table 2. Constraints on spectral transmission and reflection coefficients within filter wavelength intervals

These are the worst errors introduced by such a variation, meaning that the slope of the alteration and the position of the change are those which cause the most error. Any variations over larger intervals, for smaller changes to the spectrum, for the same change positioned across any other wavelengths within the interval, or for a change that slopes in the other direction, will lead to less error.

3.5 Camera calibration error

The errors due to the spectroradiometric calibration of the camera and its ability to measure filtered spectra accurately were measured experimentally. First, the ASR curves of the R,G and B channels were shifted slightly from Figure 4 to minimize the error in the predicted radiance for the eight filter sets shown in Table 1. This small adjustment to the ASR curves is appropriate, as it is enables absolute positioning of the ASR curves measured against known polychromatic spectra. This supplemented the initial method using monochromatic beams to position the ASR curves. The corrected ASR curves are shown in Figure 11.

§ Figure 11. Corrected absolute spectral responsivity curves

The resulting errors in radiance estimation are shown in Figure 11. These are the average error over a set of validation experiments for the preferred channel within each filter set. That is, the R, G or B channel is selected as the preferred channel for radiance estimation for each filter set depending on the sensitivity of the channel in that interval. B is the preferred channel in filter sets one through three, G is the preferred channel in sets four, five and eight, and R is the preferred channel for sets six and seven. The average error due to the camera calibration for known spectra within each filter set is less than five percent.

§ Figure 12. Average radiance estimation error for best channel among R, G and B

4. Estimating BSDFs using radiance estimates of filtered radiation

The ultimate goal of the video-goniophotometer is to measure quasi-spectral BSDFs of fenestration samples. The camera calibrations described above, enable radiance estimation for light altered by spectrally selective fenestration samples to a reasonable level of accuracy. These radiance estimates can be achieved at every pixel location in the image, which correspond to angles of

emergence from a fenestration system sample. Knowing the irradiance of the sample and the angle of incidence, quasi-spectral BSDFs can be calculated as defined in equation (1) for each filter set. These quasi-spectral BSDFs represent the average reflection or transmission coefficient of the sample for all directions across a wavelength interval.

The spectral and total irradiation of the sample and the expected, relative spectral and total radiance emerging from a neutral sample can be calculated from measured properties of the hemi-ellipsoid and the spectrum of the HMI lamp. These are used to calculate an assumed absolute responsivity of the camera for each filter set, given by:

$$(13)\quad \left[\frac{1}{h^{0.3}_{R,G,B,filterset}}\right](\theta_i,\varphi_i,\theta_{t(r)},\varphi_{t(r)}) = \sum_{filter\,interval} \frac{a_{\Delta\lambda,filterset}(\theta_i,\varphi_i,\theta_{t(r)},\varphi_{t(r)})}{h^{0.3}_{R,G,B,\Delta\lambda}}$$

Where $a_{\Delta\lambda,filterset}(\theta_i,\varphi_i,\theta_{t(r)},\varphi_{t(r)})$ is the relative spectrum of the light viewed by the camera for a given filter set. In general, $a_{\Delta\lambda,filterset}(\theta_i,\varphi_i,\theta_t,\varphi_t)$, depends on the spectral transmission or reflection coefficients of the sample. As previously shown in Table 2, however, ignoring this dependence and assuming a neutral sample across the selected wavelength interval introduces acceptable errors in radiance estimation. This responsivity can then be used in equation

(12) to calculate the radiance in each direction emerging from the sample for each filter set.

Combining the BSDFs for each filter set across the 380 to 945 nm interval leads to step-like, or quasi-spectral transmission or reflection coefficients for each direction. A sample of these quasi-spectral BSDFs, in only one direction, for four different fenestration samples is shown in Figure 13. These are simulated results which include only errors caused by the radiance estimation method, but not camera calibration errors.

§ Figure 13. Real and predicted spectral or quasi-spectral BTDF in one direction for simulated samples from Optics 5

The total, radiometric BSDF across the 380 to 1700 nm interval, including the estimate from the NIR camera, can be calculated for a given light source from the quasi-spectral BSDF as follows:

$$\mathrm{BSDF}_{e,380-1700}(\theta_i,\varphi_i,\theta_{t(r)},\varphi_{t(r)}) = \frac{\sum_{band=1}^{9}\left[\int_{band} E_{e,source}(\lambda)\cos(\theta_i)d\lambda\right]\times \mathrm{BSDF}_{e,\Delta\lambda}(\theta_i,\varphi_i,\theta_{t(r)},\varphi_{t(r)})}{\int_{380}^{1700} E_{e,source}(\lambda)\cos(\theta_i)d\lambda} \quad (14)$$

- $BSDF_{e,380-1700}(\theta_i, \varphi_i, \theta_{t(r)}, \varphi_{t(r)})$ is the total radiometric BSDF of the sample across the 380 to 1700 nm interval,
- $E_{e,source}(\lambda)$ is the spectral exitance of the source,
- $\int_{380}^{1700} E_{e,source}(\lambda)\cos(\theta_i)d\lambda$ is the total irradiance of the sample across the 380 to 1700 nm interval,
- $BSDF_{e,\Delta\lambda}(\theta_i, \varphi_i, \theta_{t(r)}, \varphi_{t(r)})$ is the radiometric BSDF across an interval $\Delta\lambda$of the sample as given by equation (1), and
- $\sum_{band=1}^{9}\left[\int_{band} E_{e,source}(\theta_i, \varphi_i, \lambda)d\lambda\right] \times BSDF_{e,band}(\theta_i, \varphi_i, \theta_{t(r)}, \varphi_{t(r)}) = L_e(\theta_i, \varphi_i, \theta_{t(r)}, \varphi_{t(r)})$ is the total radiance transmitted or reflected by the sample in direction $(\theta_{t(r)}, \varphi_{t(r)})$ for angles of incidence (θ_i, φ_i).

A total photometric BSDF can also be calculated similarly with the addition of the photopic response curve to equation (14).

A variety of real fenestration materials from the Optics 5 database[24] were simulated to verify the quasi-spectral BSDF estimation method over a range of spectral properties. They included coatings, applied films, monolithic

substrates, and laminate combinations on clear and tinted glazings. Simulations were only performed across a 380 to 945 nm interval because the HMI spectrum in the NIR region is not yet known.

For each simulation, the errors in estimated radiance for each filter set, the estimated radiance across the 380 to 945 nm wavelength interval for unfiltered radiation, and estimated luminance for unfiltered radiation were calculated. The resulting quasi-spectral BSDF for four of the simulations, for only one direction, are shown in Figure 13. The calculated errors in estimated total radiance and luminance reflected or transmitted by the sample is shown in Tables 3.

§ Table 3. Total Radiance (380-945) and Luminance Errors for Simulated Samples

The errors in total radiance or luminance are typically less than 3 percent for most of the samples. The samples that show higher errors, such as the Heat Mirror Twin Coat and Solargard Royal Blue are special cases. The 7 percent error in estimated reflected luminance and 5 percent error in reflected radiance for the Heat Mirror Twin Coat arise mainly because the reflected luminance

and radiance are so low. The 5 percent error in estimated reflected luminance for the Solargard Royal Blue sample arises mainly because of the drastically changing spectral transmission coefficients across photometrically significant wavelength intervals.

5. Conclusions

This work presents new methods for measuring radiance, luminance, and quasi-spectral, bi-directional transmission and reflection properties of fenestration systems using digital cameras. The calibrated cameras combined with color filters create a novel way for measuring the radiance and luminance of radiation with unknown spectra. The camera calibration errors introduce on average 5 percent error to the radiance estimation when the preferred channel is used. The assumed responsivity of the camera when measuring unknown spectra introduces at most 13 percent error, in the worst case, for samples with spectral properties that vary significantly over the filter intervals.

The quasi-spectral BSDFs developed using these radiance and luminance estimates recreate the gross spectral properties of fenestration samples, providing the average transmission or reflection coefficients over specified

wavebands for each direction. The total radiometric or photometric BSDFs calculated from these quasi-spectral BSDFs have been shown to be accurate to within 5 percent for most typical samples, and often much lower, neglecting camera calibration errors.

Further work has shown that these methods can be used to estimate much more accurate spectral transmission and reflection coefficients of fenestration samples. This is achieved by creating a linear system, $Ax = b$, where the radiance measured by the camera for each filter set and channel make up the vector b, A is a matrix determined by the source spectral exitance and spectral transmission and reflection coefficients of the hemi-ellipsoid, and x is a vector of the unknown transmission or reflection coefficients of the fenestration sample. A set of solutions can be found for x to estimate the spectral properties of the fenestration sample.[18]

The quasi-spectral radiance estimation method using digital cameras could also be used to measure scene radiance or luminance. Spectral transmission or reflection coefficients of surfaces in a room or differences in relative spectra of sources viewed by the camera could be deduced from the digital output of the cameras.

Acknowledgements

This work was jointly supported by the Massachusetts Institute of Technology and by the National Science Foundation under Grant No. 0533269. The authors wish to acknowledge Courtney Phillips and undergraduate students Dean Ljubicic, Zachary Clifford, Timothy Koch, Jason Ku, Keith Molina, Javier Burgos, Samuel Kronick and Danh Vo for their contributions to the device.

References

[1] USDOE. 2006 Building Energy Databook. United States Department of Energy (USDOE). Retrieved 30 April 2007, from http://buildingsdatabook.eren.doe.gov

[2] Carmody, J, Selkowitz, S, Lee, ES, Arasteh, D, Willmert, T. Window Systems for High-Performance Buildings. New York: The Regents of the University of Minnesota, 2004.

[3] Arasteh, D, Apte, J, Huang, YJ. Future Advanced Windows for Zero-Energy Homes, ASHRAE Transactions 2003; 109 Part 2.

[4] Loftness, V and Harktopf, V. Building Investment Decision Support (BIDS): Cost-Benefit Tool to Promote High Performance Components, Flexible Infrastructures and Systems Integration for Sustainable Commercial Buildings and Productive Organizations. The Austin Papers, Building Green, Inc., 2002.

[5] Boyce, PR, Hunter, C, Howlett, O. The Benefits of Daylight. Troy, NY: Lighting Research Center, Rensellear Polytechnic Institute, September 2003.

[6] Sullivan, R, Beltran, L Lee, ES; Rubin, M. and Selkowitz, SE, Energy and Daylight Performance of Angular Selective Glazings. Lawrence Berkeley National Laboratory, 1998.

[7]Beltran, LO, Mogo, BM. Assessment of Luminance Distribution Using HDR Photography: Proceedings of the 2005 ISES Solar World Congress, Orlando: International Solar Energy Society, 2005.

[8]Debevec, P and Malik, I. Recovering High Dynamic Range Radiance Maps from Photographs: Proceedings of the 24th annual conference on Computer graphics and interactive techniques. Los Angeles: Association for Computing Machinery, Inc., 1997.

[9] Andersen, M, de Boer, J. Goniophotometry and assessment of bidirectional photometric properties of complex fenestration systems. Energy and Buildings 2006; 38: 836-848.

[10] Tsuchikawa, S, Torii, M, Tsutsumi, S. Directional Characterisitics of Near Infrared Light Reflected from Wood. Holzforschung 2001; 55.5: 534-540.

[11] Baker, N, Fanchiotti, A, Steemers, K. Daylighting in Architecture. London: James & James, 1993.

[12] Breitenbach J, Rosenfeld JLJ. Design of a photogoniometer to measure angular dependent optical properties: Proceedings of International Conference on Renewable Energy Technologies in Cold Climates, Ottawa, Canada: Solar Energy Society of Canada Inc., 1998.

[13] Ward, G. Measuring and Modeling Anisotropic Reflection. Computer Graphics 1992; 26.2: 265-272.

[14] Deniel, JM, Mode´lisation des luminaires et des BRDF: re´alisation, mesure et compression, PhD thesis. Rennes : Universite´ de Rennes 1, April 2002.

[15] Andersen, M. Innovative Bidirectional Video-Goniophotometer for Advanced Fenestration Systems, PhD Thesis. Lausanne: Swiss Federal Institute of Technology, 2004.

[16] Andersen M, Gayeski N, Stokes E, Osser R, Browne C. The Heliodome project: an innovative approach in assessing solar-optical properties of light-

redirecting materials in combination with sun course simulations. Proceedings CISBAT 2007: Renewables in a changing climate - Innovation in the Built Environment. Lausanne: CISBAT, 2007.

[17] Stokes, E, Gayeski, N, Andersen, M, Estimating Spectral Information of Complex Fenestration Systems in a Video-Goniophotometer. Submitted to Lighting Research and Technology in December 2007.

[18] Clarke, TA, Fryer, JF, Wang, X. The principal point and CCD cameras, Photogrammetric Record 1998; 16(92): 293-312.

[19] Holst, G. CCD arrays, cameras and displays. SPIE Optical Engineering, 1998.

[20] Martinez-Verdu, F, Pujol, J, Bouzada, A, and Capilla, P. Spectroradiometric characterization of the spectral linearity of a conventional digital camera. Proceedings of the IS&T/SPIE Conference on Color Imaging. Scottsdale, AZ: International Society for Optical Engineering, 1999.

[21] American Society for Testing and Materials. Method E308, Standard Practice for Computing Colors of Objects by Using the CIE System. West Conshohocken, PA: ASTM International, 2001.

[22] Brown, S, Larason, T, Habauzit, C, Eppeldauer, GP, Ohno, Y, Lykke, K. Absolute Radiometric Calibration of Digital Imaging Systems. SPIE 2001; 4306: 13-21.

[23] Schott, Glass Filters Catalog. Retrieved 22 May 1007, from _http://www.us.schott.com/optics_devices/filter/english/us/index.html

[24] LBNL, Optics, Version 5.1.02. Lawrence Berkeley National Lab. Retrieved 15 Jan 2007, from http://windows.lbl.gov/materials/optics5/CurrentVersion/Release%20notes.htm

LIST OF TABLES

Table 1. Filter Specifications

WAVELENGTH INTERVAL	SCHOTT COLOR GLASS FILTERS AND THICKNESSES
1) 380-500 nm	GG400 (1 mm), BG25 (2 mm),BG39 (1mm)
2) 450-590 nm	GG455 (2 mm), BG7 (2 mm)
3) 480-590 nm	GG495 (2 mm), BG 7 (2 mm)
4) 500-650 nm	OG530 (2 mm), BG42 (2 mm)
5) 550-640 nm	OG570 (2 mm), BG39 (2 mm)
6) 570-690 nm	OG590 (2 mm), BG40 (2 mm)
7) 650-850 nm	RG665 (2 mm), KG1 (2 mm)
8) 800-945 nm	RG830 (2 mm)

Table 2. Constraints on spectral transmission and reflection coefficients within filter wavelength intervals

Parameter/Filter Set	**F1**	**F2**	**F3**	**F4**	**F5**	**F6**	**F7**	**F8**
Filter Start Wavelength(nm)	380	450	480	500	550	570	650	800
Filter End Wavelength(nm)	500	590	590	650	640	690	850	945
Variation interval (nm)	50	100	50	50	50	50	100	100
Percent Change in R or T	35	30	50	35	30	50	30	50
Max Rad. Error	10	9	9	13	13	6	5.5	13
Max Lum. Error	19	24	9	9	7	21	N/A	N/A

Table 3. Total Radiance (380-945) and Luminance Errors for Simulate Samples

Sample	**Total Radiance Error (%)**	**Total Luminance Error (%)**
SolarGard@SilverAG25 LowE	0.19	0.39
Panorama Autumn Bronze 30	1.52	0.31
Solis Clear on Clear	2.21	1.69
Pewter on Clear	0.20	0.08
Heat Mirror Twin Coat	4.98	6.94
Sea Storm	2.06	0.18
Solargard Royal Blue	2.65	5.30
Armourglass Greylight	0.78	2.52
Vanceva	1.10	0.11
Azurelite	2.52	0.31

LIST OF FIGURES

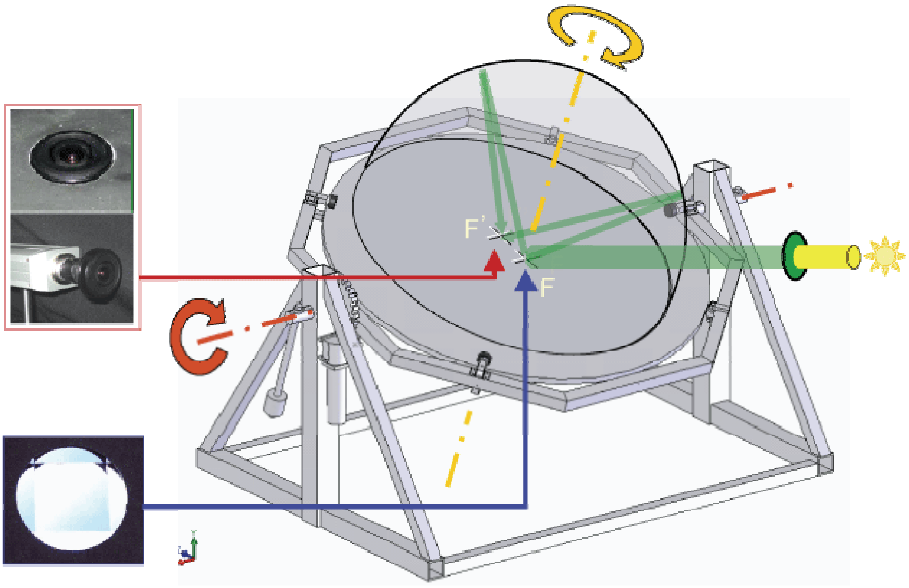

Figure 1. MIT video-goniophotometer

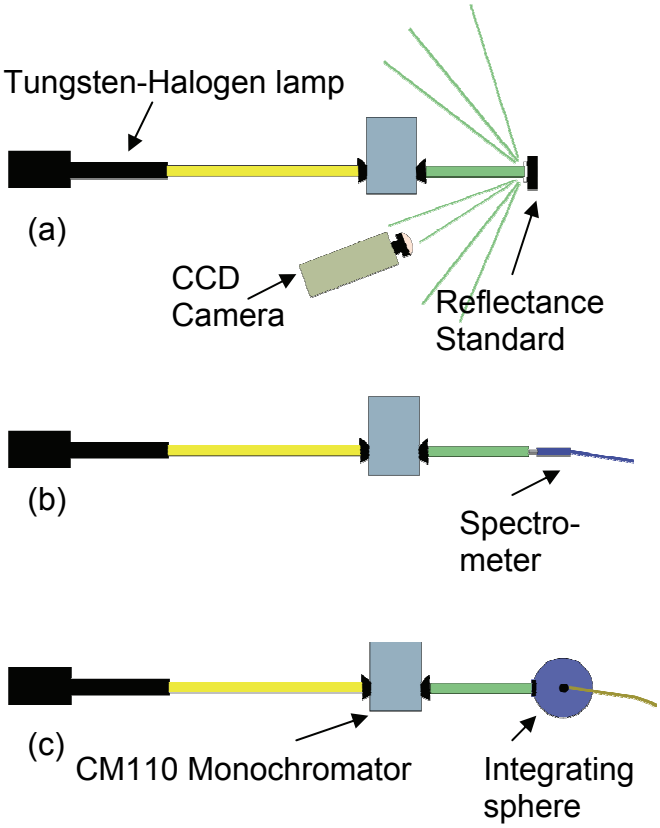

Figure 2. Spectroradiometric experimental schematic
(a) Images taken with CCD camera
(b) Monochromatic irradiance measured with spectrometer
(c) Monochromatic irradiance measured with integrating sphere

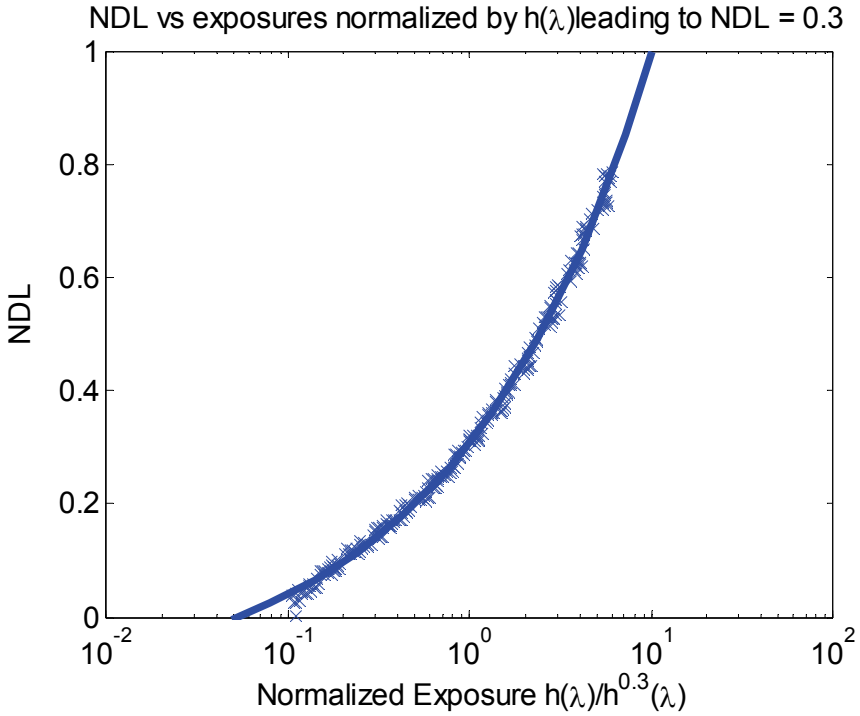

Figure 3. Normalized response for R, G and B channels to many wavelengths fit with a logistic dose response function

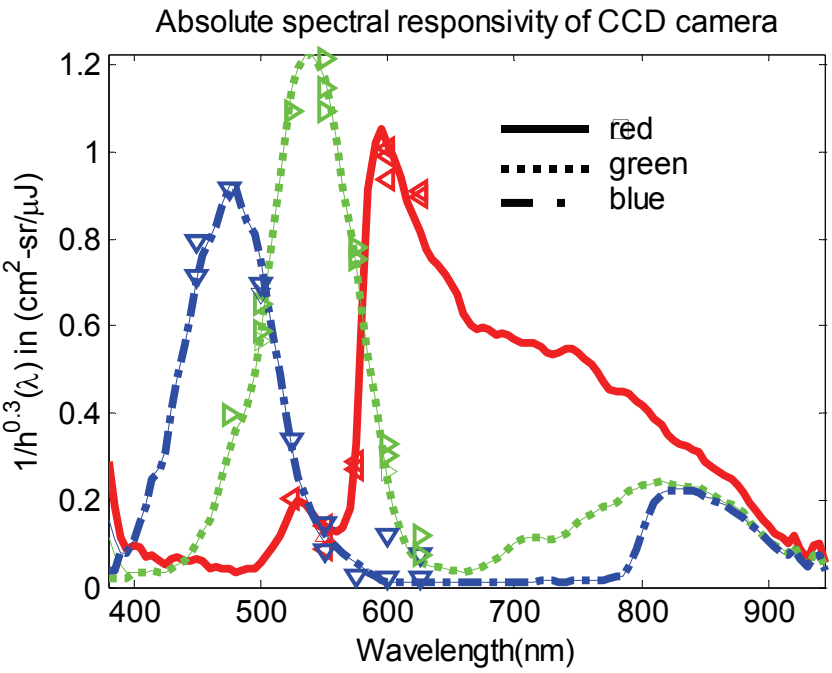

Figure 4. Absolute spectral responsivity curves for R, G and B channels scaled to integrating sphere calibration points

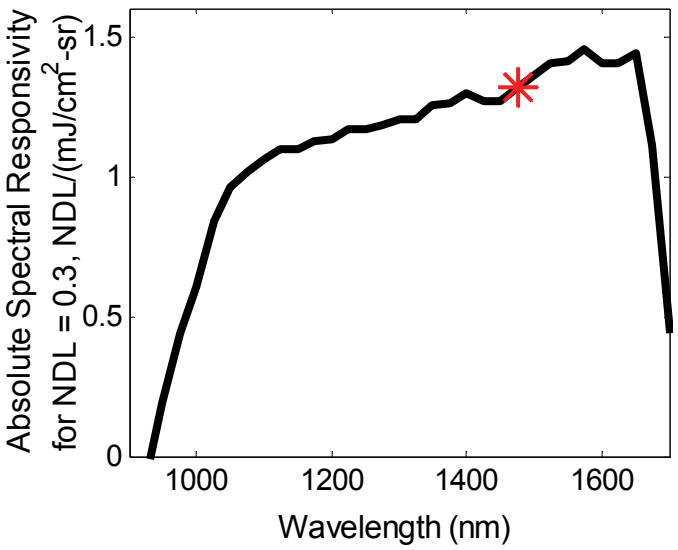

Figure 5. Absolute spectral responsivity of the InGaAs camera

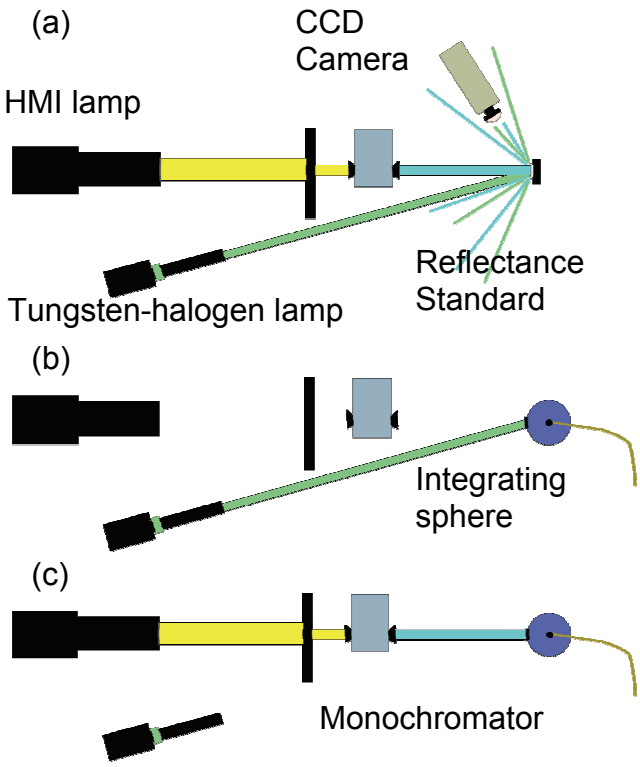

Figure 6. Schematic of the two beam polychromatic response experiment
(a) Camera viewing polychromatic radiance generated by 500 and 550 nm beams irradiating a reflectance standard
(b) Measuring the irradiance of the reflectance standard from the 550 nm beam using the integrating sphere and
(c) the same for the 500 nm beam

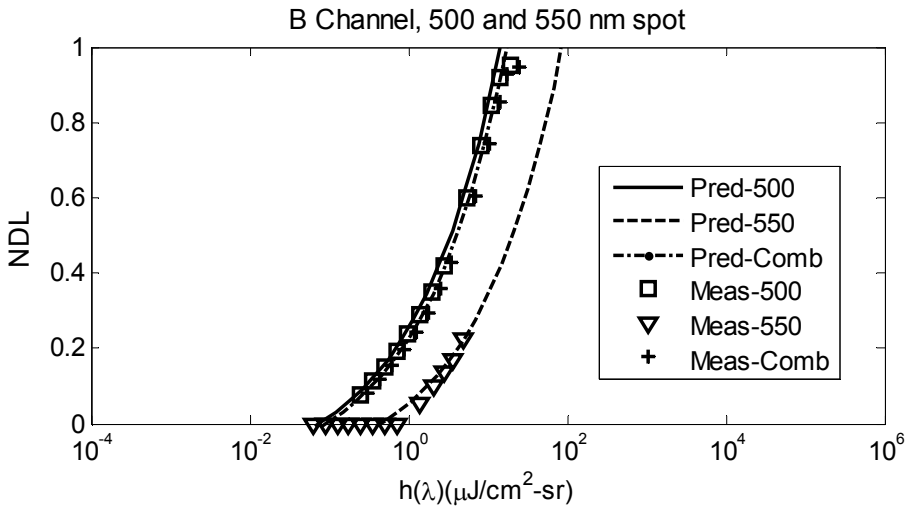

Figure 7. Two beam polychromatic experiment results: predicted exposures (Pred) from B channel compared to measured exposures (Meas) for two separate beams (500, 550) and a polychromatic beam (Comb)

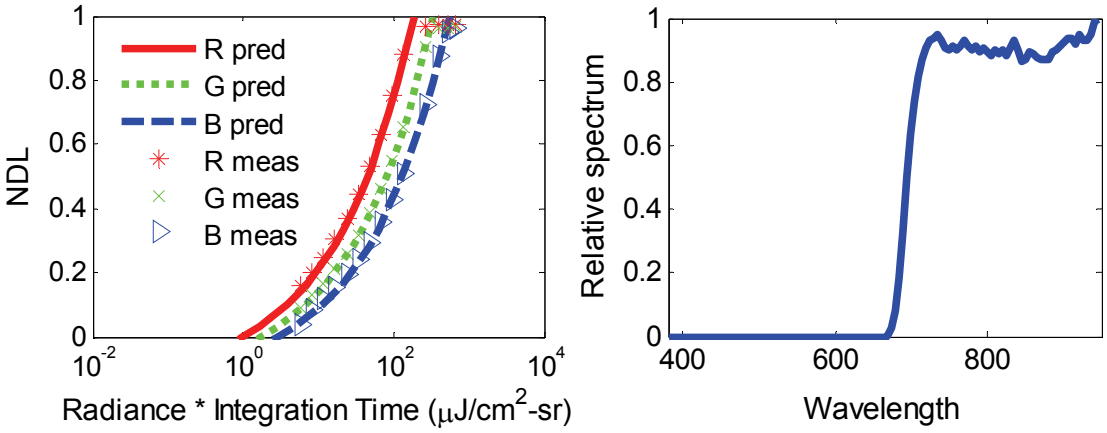

Figure 8. General polychromatic response: camera response to tungsten-halogen lamp with 695 nm long pass filter

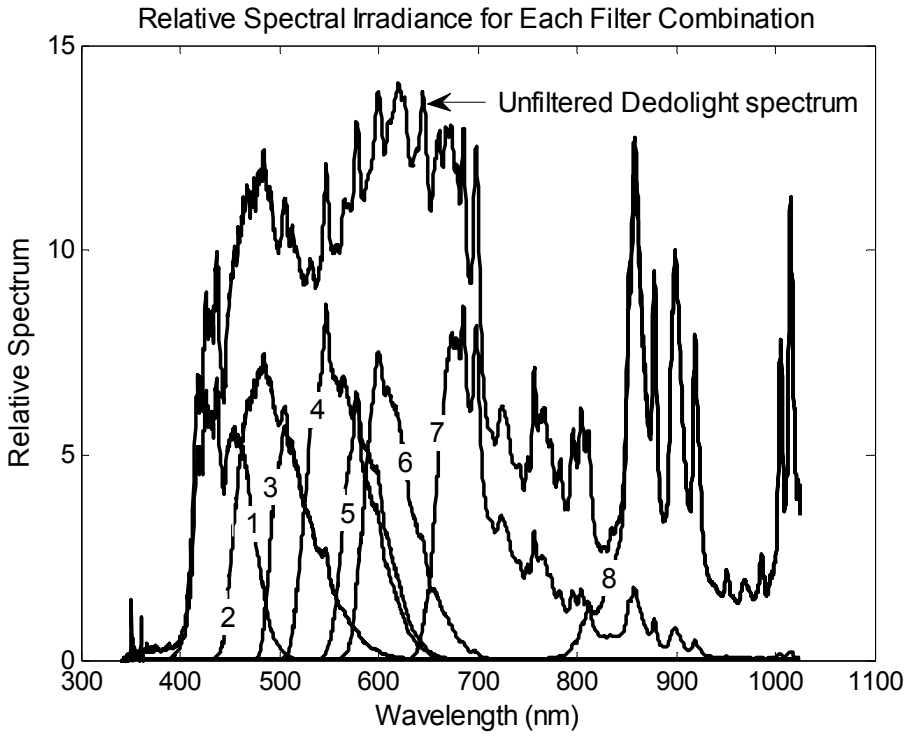

Figure 9. Unfiltered HMI lamp spectrum and the filtered HMI lamp spectra for each of the eight filter combinations listed in Table 1

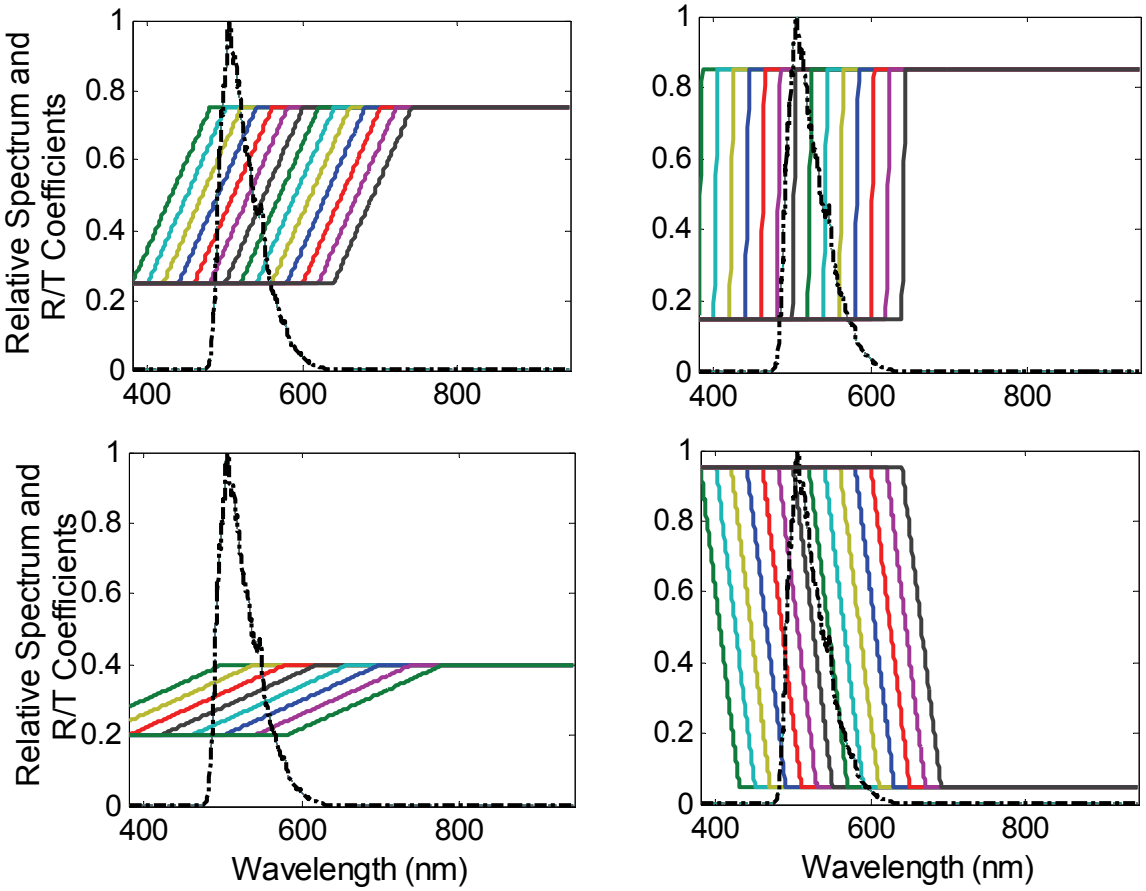

Figure 10. The effect of linearly varying hypothetical transmission coefficients, shifted across the filtered spectra, were studied to calculate the theoretical accuracy of using each filter set to estimate radiance and luminance across a given band.

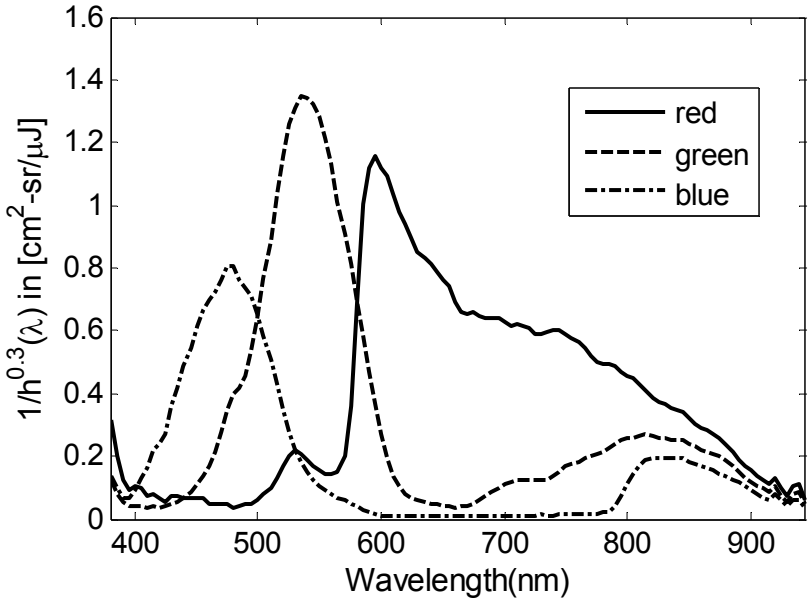

Figure 11. Corrected absolute spectral responsivity curves

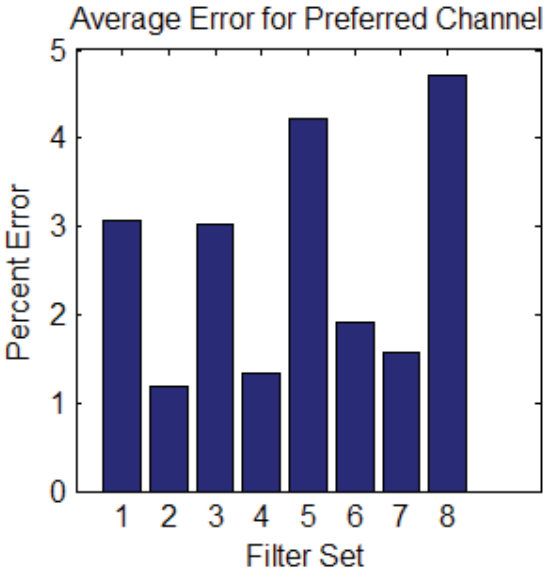

Figure 12. Average radiance estimation error for best channel among R, G and B

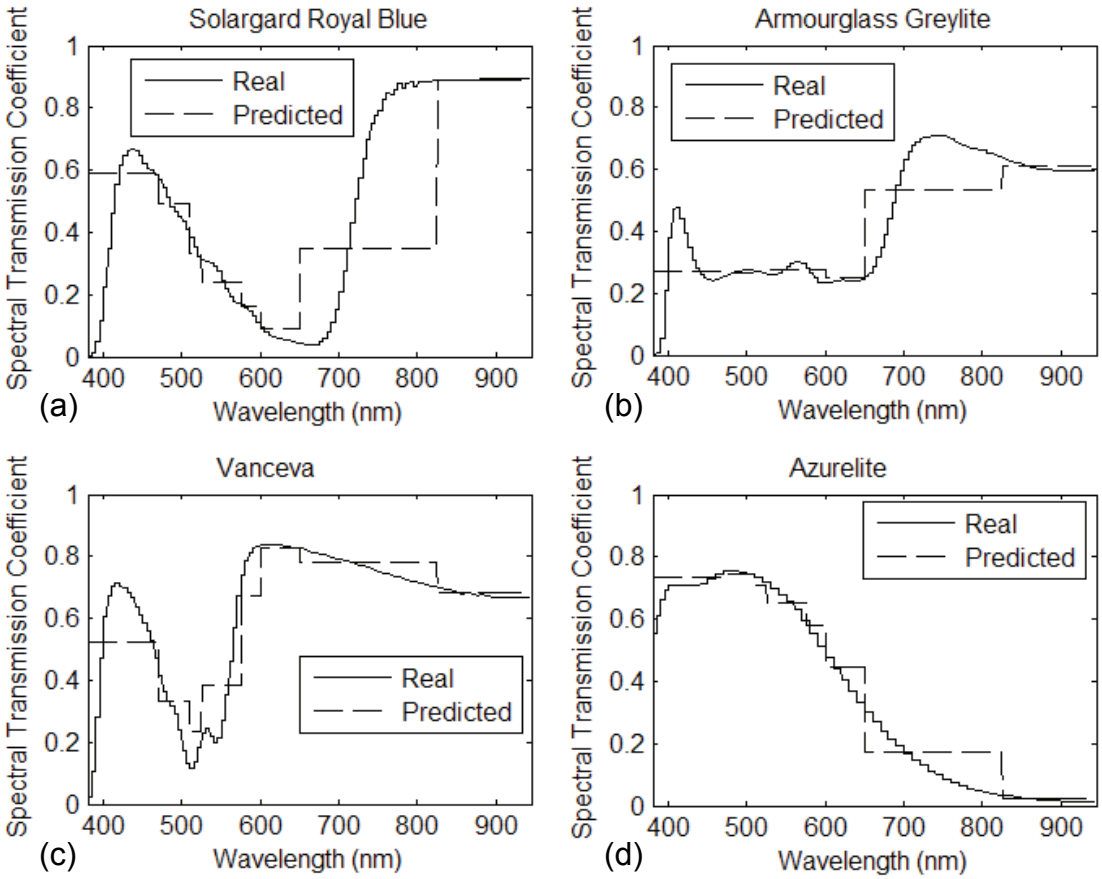

Figure 13. Real and predicted spectral or quasi-spectral BTDF in one direction for simulated samples from Optics 5